New Journal of Physics
The open access journal at the forefront of physics

Deutsche Physikalische Gesellschaft DPG
IOP Institute of Physics

Published in partnership with: Deutsche Physikalische Gesellschaft and the Institute of Physics

OPEN ACCESS

RECEIVED
21 February 2016

REVISED
22 June 2016

ACCEPTED FOR PUBLICATION
8 July 2016

PUBLISHED
12 August 2016

PAPER

Observation of topological Hall effect in Mn_2RhSn films

K G Rana[1,2], O Meshcheriakova[2], J Kübler[3], B Ernst[2], J Karel[2], R Hillebrand[1], E Pippel[1], P Werner[1], A K Nayak[1,2], C Felser[2] and S S P Parkin[1]

[1] Max Planck Institute of Microstructure Physics, Weinberg 2, D-06120 Halle, Germany
[2] Max Planck Institute for Chemical Physics of Solids, Nöthnitzer Str. 40, D-01187 Dresden, Germany
[3] Institut für Festkörperphysik, Technische Universität Darmstadt, D-64289 Darmstadt, Germany

E-mail: stuart.parkin@mpi-halle.mpg.de

Keywords: spintronics, Heusler, Hall effect

Abstract

Recently non-collinear magnetic structures have attracted renewed attention due to the novel Hall effects that they display. In earlier work evidence for a non-collinear magnetic structure has been reported for the ferromagnetic Heusler compound Mn_2RhSn. Using sputtering techniques we have prepared high quality epitaxial thin films of Mn_2RhSn by high temperature growth on MgO (001) substrates. The films are tetragonally distorted with an easy magnetization axis along the *c*-axis. Moreover, we find evidence for an anomalous Hall effect whose magnitude increases strongly below the Curie temperature that is near room temperature. Consistent with theoretical calculations of the anomalous Hall conductivity that we have carried out by deriving the Berry curvature from the electronic structure of perfectly ordered Mn_2RhSn, the sign of the anomalous Hall conductivity is negative, although the measured value is considerably smaller than the calculated value. We attribute this difference to small deviations in stoichiometry and chemical ordering. We also find evidence for a topological Hall resistivity of about 50 nΩ cm, which is ~5% of the anomalous Hall effect, for temperatures below 100 K. The topological Hall effect signifies the presence of a chiral magnetic structure that evolves from the non-collinear magnetic structure that Mn_2RhSn is known to exhibit.

1. Introduction

Magnetic non-collinear spin textures, such as magnetic bubbles and skyrmions [1–10], have recently attracted much attention, both from a fundamental as well as a technological perspective. Whilst magnetic bubbles were extensively studied several decades ago as non-volatile magnetic bits in magnetic bubble memory devices, renewed interest in bubbles and related skyrmions arises from the possibility of manipulating these magnetic nano-objects using electrical currents via spin transfer torques [9, 11–14]. Skyrmions, predicted theoretically many years ago [3, 15], have recently been experimentally detected in various materials including single crystals of MnSi via small angle neutron scattering [11], and FeGe via Lorentz transmission electron microscopy (TEM) [6]. In these systems lattices of skyrmion are formed when there is a sufficiently large Dzyaloshinskii–Moriya indirect exchange interaction (DMI) compared to the direct Heisenberg exchange [16, 17]. A DMI exchange requires an absence of inversion symmetry, which can also take place at interfaces: recently skymions have been observed in various magnetic thin films deposited on underlayers with sufficiently large DMI [18], but in most cases magnetic fields are required to stabilize skyrmions or the skyrmions are found only at low temperatures. Heusler compounds are a large family of compounds that offer tunability in many key parameters that are needed to engineer novel magnetic states [19]. Heuslers have the general chemical formula X_2YZ, where X and Y are transition metals, and Z is a main group element. Heuslers with X = Mn have high Curie temperatures. These compounds crystallize in either an inverse cubic or a tetragonal structure when Y is a late transition metal element. Since the DMI interaction originates from spin–orbit coupling, the DMI interaction is typically larger for heavy elements. Thus, the Mn_2RhSn system [20, 21] is of especial interest. Mn_2RhSn has two magnetic sub-lattices, with alternating planes of Mn_I and Mn_{II} moments that prefer an anti-parallel arrangement. Mn_I

moments are fixed and oriented along the *c* axis but the Mn_{II} moments face competing nearest and next nearest neighbor antiparallel coupling that can lead to canted moments [20].

Neutron diffraction studies of bulk polycrystalline Mn_2RhSn have revealed a canting of Mn_{II} moments below a spin reorientation transition near ~80 K [20]. Electronic properties, studied by hard x-ray photoelectron spectroscopy, and the temperature dependence of magnetoresistance in thin films of Mn_2RhSn have been studied by Meshcheriakova *et al* [21]. In this work, we report the observation of a temperature dependent topological Hall effect (THE) in thin films of Mn_2RhSn. The origin of THE is discussed in terms of an additional component to the Berry phase caused by the non-collinear spin arrangement in the Mn_2RhSn. Our study is relevant for stabilizing magnetic sub-structures such as skyrmions in Heusler thin films, where T_C can be tuned to well above room temperature.

2. Experimental details

Thin films of Mn_2RhSn were grown on MgO (001) substrates at 350 °C using DC magnetron co-sputtering from Mn, Rh and Sn sputter targets. To improve chemical ordering, the films were annealed at the growth temperature for 30 min The annealed films were capped *in situ* with ~3 nm thick MgO films that were deposited at room temperature. The film composition was characterized using energy-dispersive x-ray (EDX) microscopy. Structural characterization was carried out using standard x-ray diffractometry using CuK_α radiation ($\lambda = 1.5406$ Å). Magnetization measurements were performed with a vibrating sample magnetometer (MPMS 3, Quantum Design). Transport measurements were carried out in a Quantum Design Dynacool system.

3. Results and discussions

3.1. Structural characterization

Figure 1(a) shows x-ray diffraction patterns for a 40 nm thick Mn_2RhSn film grown on an MgO (001) substrate and post-annealed at 350 °C. A tetragonal structure is confirmed from the diffraction peak positions. As shown in the schematic diagram of the unit cell in the inset to figure 1(a), the Mn atoms occupy two different lattice sites. Mn_I have a tetragonal coordination and occupy 2b (0, 0, 1/2) Wyckoff positions. Mn_{II} have an octahedral coordination and occupy 2c (0, 1/2, 1/4) Wyckoff positions. Rh atoms occupy 2d (0, 1/2, 3/4) and Sn atoms occupy 2a (0, 0, 0) Wyckoff positions [22]. 2θ-ω scans were obtained to find (00n) and (112) peaks by an appropriate sample alignment: typical scans are shown in figure 1(a) and its inset, respectively. The out-of-plane (OP) (c) and the in-plane (IP) (a) lattice parameters are thereby determined to be 6.50 ± 0.01 Å and 4.30 ± 0.01 Å, respectively. Thus the c/a ratio is found to be 1.51 which is consistent with a tetragonal structure. These values compare with those of 6.62 Å and 4.29 Å found for bulk material [22]. Strain due to lattice mismatch of the thin films with the MgO (001) substrate (4.21 Å) likely accounts for the difference in values between the thin films and bulk, although small differences in composition and in the chemical ordering could also be responsible. The surface topography of the thin films was analyzed by atomic force microscopy (AFM). Figure 1(b) shows an AFM scan for an area of $3\ \mu m \times 3\ \mu m$ of a 40 nm thick film: a r.m.s roughness of 0.6 nm is obtained. TEM was performed to evaluate the film quality at the nanoscale. Figure 1(c) shows an overview of a cross-sectional TEM of a 40 nm thick film. High quality single crystalline thin film growth is observed. A high resolution TEM image shown in figure 1(d) shows the epitaxial nature of the film grown on the MgO substrate. The inset shows a higher magnification image with over-laid calculated atomic positions in the (100) zone-axis orientation, confirming the tetragonal structure of the film. EDX analysis shows the stoichiometry of the film to be $Mn_{52.63\pm.70}\,Rh_{21.77\pm0.3}Sn_{25.60\pm0.33}$.

3.2. Magnetic properties

The temperature dependence of the magnetization (M) of a 56 nm thick film with $\mu_o H = 0.1$ T parallel to the *c* axis (out-of-plane, OP) is shown in figure 2(a). The Curie temperature (T_C) is determined to be 293 ± 4 K by taking the first derivative of the temperature dependence of the magnetization curve. The resulting T_C is close to that of 270 K reported earlier for stoichiometric bulk polycrystalline samples [22]: the T_C in these earlier studies was found to depend sensitively on the composition of the material so the slightly higher T_C that we find in our thin films is likely due to small variations away from the nominal stoichiometry, as indicated by EDX analysis mentioned above.

The magnetization measurements were performed in zero field cooled (ZFC, black solid curve) and field cooled (FC, red solid curve) conditions. The difference in the ZFC and FC curves at low temperatures presumably arises due to the unsaturated magnetic state in the ZFC curve as a result of the high magnetic anisotropy of the tetragonal phase. As expected, the (IP ZFC and FC M versus T curves exhibit a smaller magnetization than that of the OP curves due to the higher magnetic fields required to saturate the

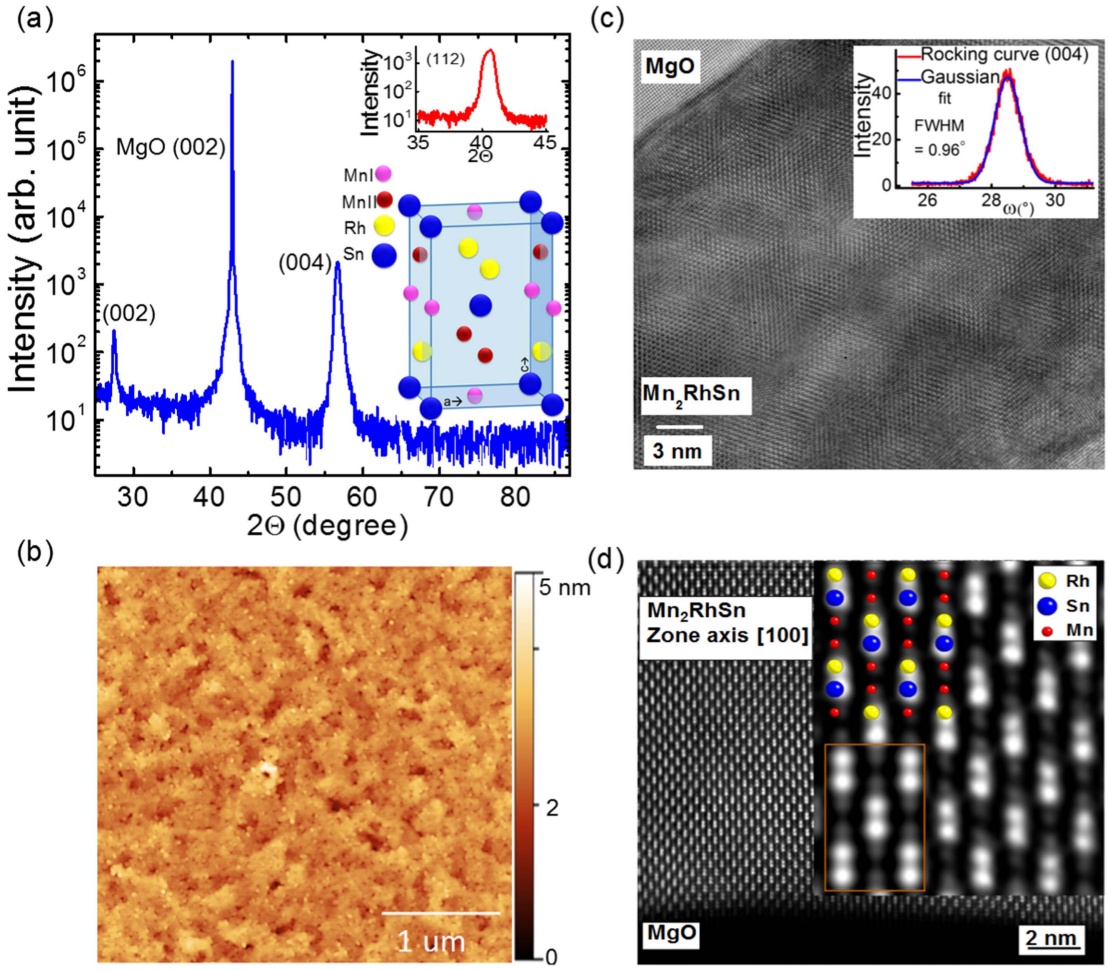

Figure 1. Characterization of sputter deposited Mn_2RhSn films grown on single crystalline MgO (001). (a) X-ray θ-2θ diffraction pattern for a 40 nm thick film shows the expected (00n) single crystalline peaks as shown. From the (004) and (002) peaks, the out-of-plane lattice parameter $c = 6.50 \pm .01$ Å. From the (112) peak, shown by the red solid curve in the inset, the in-plane lattice parameter was found to be 4.30 ± 0.01 Å, confirming that the film has a tetragonal structure. (b) AFM image that indicates a root mean square (r.m.s) roughness of ~0.6 nm for a 40 nm thick Mn_2RhSn thin film. The inset in (c) shows the rocking curve of the (004) reflection performed by varying ω in the (100) plane at fixed 2θ. The full width at half maxima (FWHM) is 0.96°. (c) Low magnification cross-sectional transmission electron microscopy (XTEM) image of a 40 nm thick film with a 2.5 nm thick crystalline MgO capping layer. (d) High resolution XTEM image shows the epitaxial nature of the film grown on the MgO substrate. The inset shows a higher magnification image with over-laid calculated atomic positions along the (100) zone-axis orientation, confirming the tetragonal structure of the film.

magnetization IP. This is confirmed by magnetic hysteresis loops that were obtained at various temperatures after zero field cooling the samples from a temperature above T_C. The OP and IP hysteresis loops measured at 50 K are shown in figure 2(b). It can be clearly seen that the easy axis of magnetization is along the *c*-axis. The saturation field along the *c* axis is much smaller ($\mu_o H_S \sim 0.3$ T), than IP ($\mu_o H_S \sim 1.1$ T). The coercivities for the OP and IP hysteresis loops are ≈0.06 T and ≈0.026 T at 50 K, respectively. The coercivities vanish near T_C. For both cases a saturation magnetization (M_S) of nearly 1.6 μ_B f.u. is obtained at 5 T. The OP hysteresis loops taken at different temperatures are shown in figure 2(c). H_C^{OP} systematically decreases with increasing temperature and disappears at T_C. From the hysteresis obtained for $H \parallel c$ and $H \perp c$, the magnetic anisotropy is calculated using the equation below

$$K_u = \frac{1}{2} H_k \mu_0 M_s, \tag{1}$$

K_u is the effective uniaxial OP anisotropy energy. The anisotropy field $\mu_0 H_k$ is found to be 1.1 T from figure 2(b), thus K_u is calculated to be 0.14 MJ m^{-3} at 50 K. The zero field cooled virgin magnetization curves measured at various temperature are shown in figure 2(d).

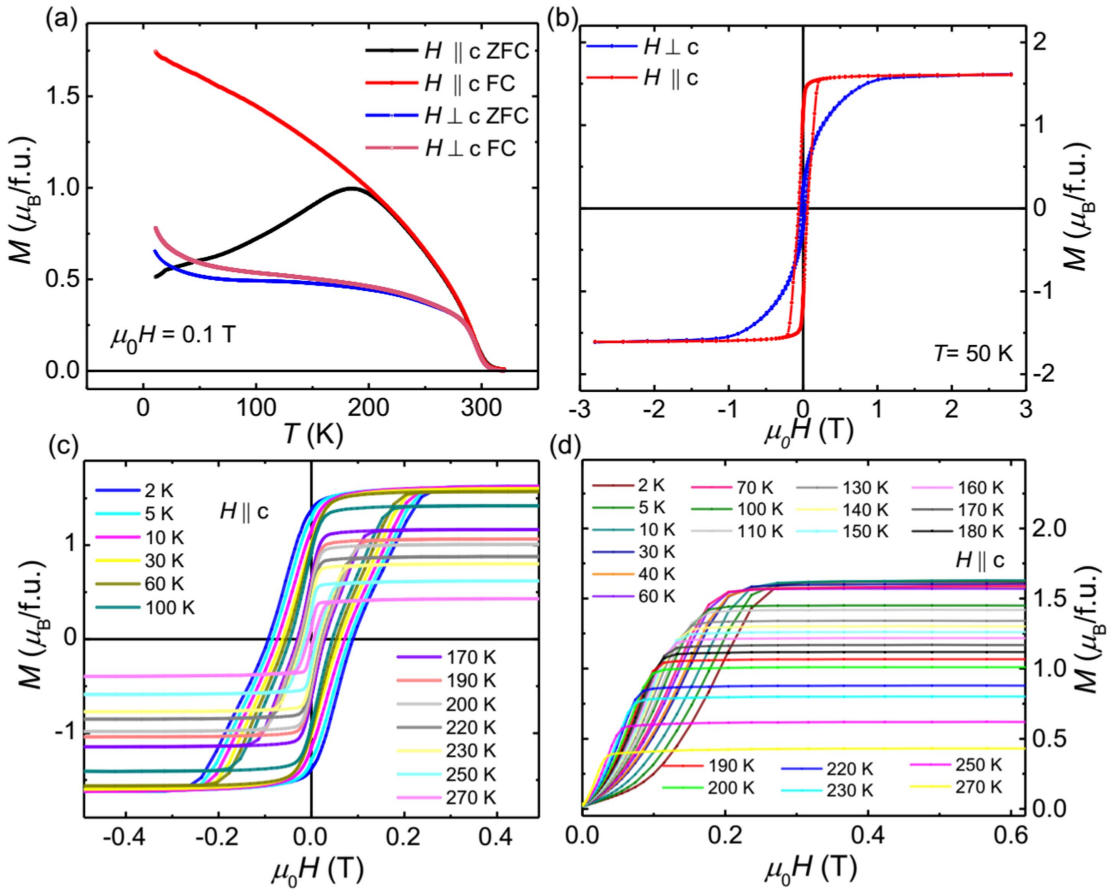

Figure 2. Magnetic properties of a 56 nm thick Mn_2RhSn film: (a) temperature dependence of the magnetization for $H \| c$ (OP) and $H \perp c$ (IP) measured at 0.1 T. The ferrimagnetic phase sets in below 290 K (T_C) and clearly shows the OP magnetized state of the films. (b) Magnetic hysteresis loops at 50 K for the zero field cooled state: red curve: OP, and, blue curve: IP, that shows that the easy axis of magnetization is OP with a saturation field, $\mu_0 H_S \sim 0.3$ T. The corresponding IP value is 1.1 T. The OP coercivity ($\mu_0 H_C^{OP}$) is ≈0.06 T. (c) Magnetic hysteresis loops measured at various temperatures for $H \| c$. (d) The virgin curves measured at various temperatures after performing a zero field cool at each temperature show a decrease in M_S and H_C^{OP} that finally vanish above T_C.

4. Hall effect measurements

Non-collinear magnetic structures can give rise to an additional Hall resistance [10]. Hall resistivity (ρ_{xy}) was measured for several Mn_2RhSn thin films for temperatures between 2 and 290 K using the experimental setup shown schematically in figure 3(a). An IP current was applied along the x-axis, the magnetic field was applied parallel to the z-axis (c) and the Hall voltage (V_H) was measured along the y-axis using fields up to 5 T. Since the dependence of R_{xx} on magnetic field is negligible (figure 3(a)), so to eliminate the R_{xx} contribution, we have offset the raw R_{xy} at zero field to zero at each temperature. Typical data are shown in figure 3(b). Each measurement was performed after ZFC. ρ_{xy} is found to be ~ -1 $\mu\Omega$ cm at 2 K which is considerably higher than found in earlier studies on similarly prepared films although these earlier films were protected by a 5 nm thick Rh layer which would shunt current [21]. ρ_{xy} increases nonlinearly for low fields and linearly for $\mu_o H > 0.3$ T. The low field nonlinear behavior is enhanced for $T < 100$ K. To determine the origin of this nonlinear part of ρ_{xy} we have used the following relationship

$$\rho_{xy} = R_o H + \rho^{AHE} + \rho^{THE}, \tag{2}$$

where $R_o H$, ρ^{AHE}, and ρ^{THE} correspond to the ordinary, anomalous (AHE) and topological Hall effects, respectively. $R_o H$ is obtained by a linear fit of ρ_{xy} between 1 and 5 T as shown in the inset of figure 3(c). The AHE has contributions from intrinsic and extrinsic scattering mechanisms as follows

$$\rho^{AHE} = (\alpha \rho_{xx}^2 + \beta \rho_{xx}) M, \tag{3}$$

where, ρ_{xx} is the longitudinal resistivity and the term with α corresponds to intrinsic and side-jump scattering whereas the term with β corresponds to skew scattering. At a fixed T, ρ_{xx} has a very weak dependence on the magnetic field (shown in figure 3(a)), hence ρ^{AHE} effectively depends linearly on M. ρ^{THE} is the contribution from any chiral spin texture present in the material and for $H > H_C$, ρ^{THE} is expected to be zero. Hence, for

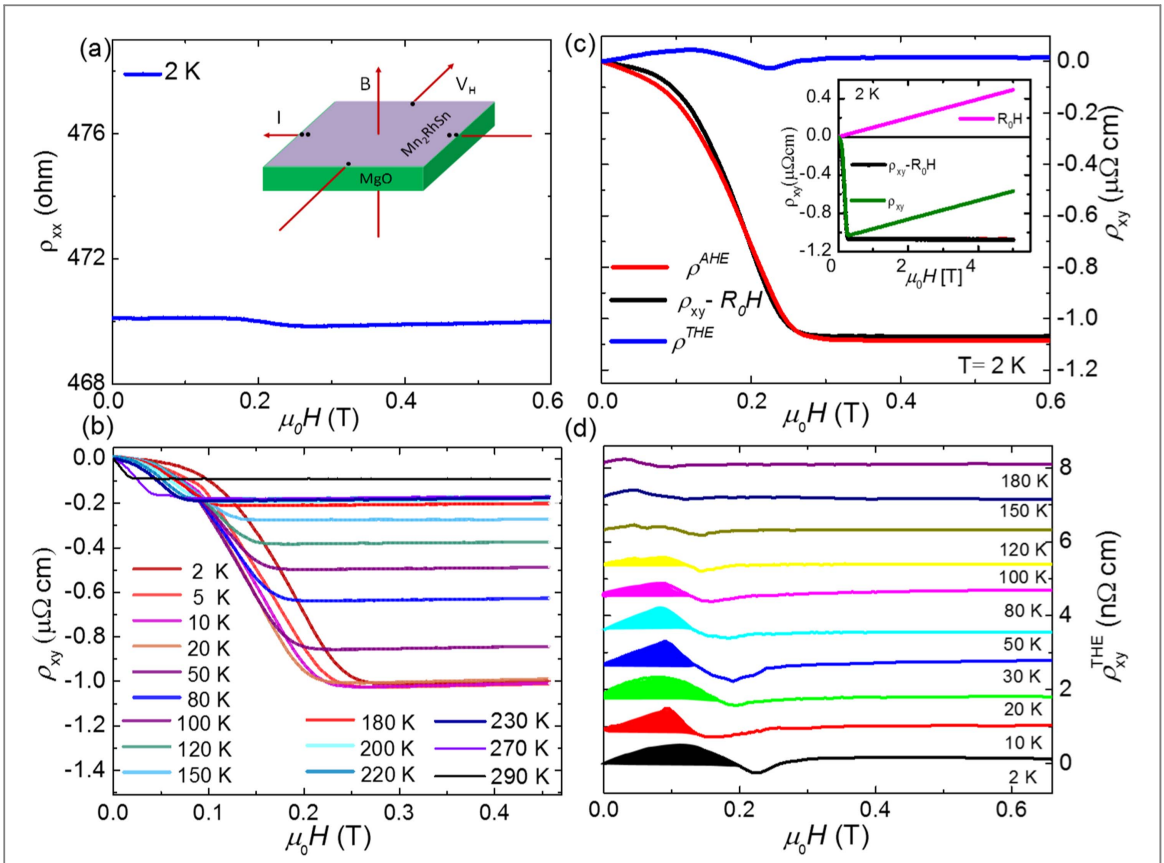

Figure 3. (a) The inset shows the measurement schematic for the four wire resistance and Hall resistance measurements. The magnetic field is applied perpendicular to the plane of the film i.e. *H*||*c*. The Hall voltage V_H is measured in the transverse direction to that of the current. The full film is used for these measurements where the contacts are made to the film using aluminum wire bonding, as indicated with black dots in the inset. The blue solid line shows the longitudinal resistivity as a function of magnetic field at 2 K. (b) Hall resistance measured at various temperatures between 2 and 290 K after zero field cooling. (c) The inset shows the ordinary Hall component is extracted from ρ_{xy} and the difference is represented by the black solid line for $T = 2$ K. The topological Hall effect is extracted from hall resistance. The red solid line corresponds the anomalous Hall effect, calculated from the magnetization data and longitudinal resistivity. Blue solid line therefore corresponds to the topological Hall effect contribution (ρ^{THE}) calculated by subtracting the the curves. (d) ρ^{THE} at few selected temperatures in the range 2–290 K. ρ^{THE} is zero for all temperatures above 100 K. Upon cooling, ρ^{THE} appears at 100 K and increases until the lowest measured temperature of 2 K.

$H > H_C$, $(\rho_{xy} - R_oH)$ is fitted to each contribution as in equation (3). In figure 3(c) the black solid curve corresponds to $(\rho_{xy} - R_oH)$ and the red solid curve is ρ^{AHE} obtained at $T = 2$ K. A non-zero value of ρ^{THE} is obtained at low fields ($H < H_C$), and is shown by the blue solid curve. A maximum of ρ^{THE} at 2 K is about 50 nΩ cm and is nearly 5% of the total AHE. We have performed a similar analysis for all measured temperatures and found that ρ^{THE} almost disappears for temperatures above 100 K. The magnitude of ρ^{THE} observed in Mn_2RhSn is slightly higher than that found in MnSi [10]. The topological Hall component observed in the present case indicates the presence of a non-collinear spin structure below 100 K which is also observed by neutron diffraction experiments [20]. The finding of such a THE in other materials has been attributed to the presence of chiral magnetic structures such as skyrmions [10]. Thus the observation of a THE in Mn_2RhSn thin films is evidence for the presence of a chiral magnetic structure. We have observed similar results in similarly grown samples, however a further systematic investigation on thickness and stoichiometry is suggested.

5. AHE calculation

The band-structure and the Berry-curvature of Mn_2RhSn was computed using the ASW (LMTO) method [23, 24]. The standard local spin-density functional approximation was used. The magnetic structure considered in these calculations was a non-collinear ferromagnetic, as described before [20]. The results obtained are interesting in the details of the Berry-curvature pattern [24]. In figure 4 this is shown in two planes symmetric with respect to the plane through $k = 0$. One recognizes a rotation of the pattern by $\pi/2$; this rotation does not lead to canceling contributions in opposite parts of the Brillouin zone but is summed up to give the anomalous Hall conductivity having a value of $\sigma_{xy} = -184\ (\Omega\text{cm})^{-1}$. To obtain the Hall resistivity one needs the longitudinal resistivity ρ_{xx} for which we measured a value of ~470 μΩ cm at 2 K. An experimental value of σ_{xy} is

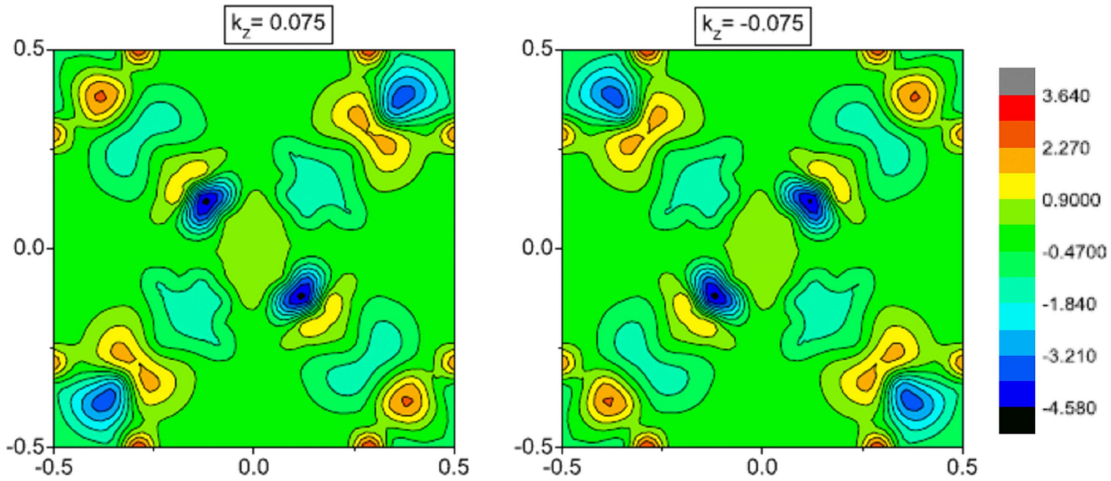

Figure 4. Berry curvature in two planes cut through the Brillouin zone normal to the k_Z axis. The values given are in units of e^2/h.

then obtained to be $-4.8\ (\Omega\text{cm})^{-1}$ by using

$$\sigma_{xy} = \frac{\rho_{xy}}{\rho_{xx}^2}, \tag{4}$$

which is valid for $\rho_{xx} \gg \rho_{xy}$. However, the measured value is much smaller than the calculated value, presumably because of the rather large value of the longitudinal resistivity (see the significantly smaller ρ_{xx} in [21]). In a similar way as for σ_{xy}, we also calculate values of σ_{yz} and σ_{zx} which are found to be around $-8\ (\Omega\text{cm})^{-1}$, and much smaller than σ_{xy}. The anomalous Hall conductivity calculation is performed for a perfect single crystal, perfectly ordered and at 0 K. From the x-ray diffraction, discussed above, we find a FWHM of ~0.96° for the rocking curve obtained from the (004) peak, indicating the degree mosaicity in the films. Furthermore, the possibility of stoichiometric variations in our films cannot be completely ignored. These factors might account for the low values of the measured Hall conductivities. But the rather high value of the longitudinal resistivity could also be a result of these factors.

6. Conclusion

We find evidence of a significant anomalous Hall conductivity in thin single crystalline films of the Heusler compound Mn_2RhSn below its Curie temperature, whose sign is consistent with theoretical calculations. Below ~100 K evidence for a small THE is found that is indicative of a chiral or helical magnetic ordering beyond a simple non-collinear magnetic ordering.

Acknowledgments

Partial support from the European Research Council Advanced Grant No. 291472 'IDEA-HEUSLER (Claudia Felser) and No. 670166 'SORBET' (Stuart Parkin) is gratefully acknowledged.

References

[1] Bogdanov A N and Rößler U K 2001 Chiral symmetry breaking in magnetic thin films and multilayers *Phys. Rev. Lett.* **87** 037203
[2] Bogdanov A N, Rößler U K, Wolf M and Müller K H 2002 Magnetic structures and reorientation transitions in noncentrosymmetric uniaxial antiferromagnets *Phys. Rev.* B **66** 214410
[3] Rößler U K, Bogdanov A N and Pfleiderer C 2006 Spontaneous skyrmion ground states in magnetic metals *Nature* **442** 797–801
[4] Ulrich K R, Andrei A L and Alexei N B 2011 Chiral skyrmionic matter in non-centrosymmetric magnets *J. Phys.: Conf. Ser.* **303** 012105
[5] Wilson M N *et al* 2013 Discrete helicoidal states in chiral magnetic thin films *Phys. Rev.* B **88** 214420
[6] Yu X Z *et al* 2010 Real-space observation of a two-dimensional skyrmion crystal *Nature* **465** 901–4
[7] Heinze S *et al* 2011 Spontaneous atomic-scale magnetic skyrmion lattice in two dimensions *Nat. Phys.* **7** 713–8
[8] Yu X Z *et al* 2011 Near room-temperature formation of a skyrmion crystal in thin-films of the helimagnet FeGe *Nat. Mater.* **10** 106–9
[9] Yu X Z *et al* 2012 Skyrmion flow near room temperature in an ultralow current density *Nat. Commun.* **3** 988
[10] Li Y *et al* 2013 Robust formation of skyrmions and topological Hall effect anomaly in epitaxial thin films of MnSi *Phys. Rev. Lett.* **110** 117202
[11] Muhlbauer S *et al* 2009 Skyrmion lattice in a chiral magnet *Science* **323** 915–9
[12] Seki S, Yu X Z, Ishiwata S and Tokura Y 2012 Observation of skyrmions in a multiferroic material *Science* **336** 198–201

[13] Jonietz F et al 2010 Spin transfer torques in MnSi at ultralow current densities Science 330 1648–51
[14] Schulz T et al 2012 Emergent electrodynamics of skyrmions in a chiral magnet Nat. Phys. 8 301–4
[15] Bogdanov A N and Yablonskii D A 1989 Thermodynamically stable 'vortices' in magnetically ordered crystals. The mixed state of magnets J. Exp. Theor. Phys. 68 101–3
[16] Dzyaloshinskii I E 1957 Thermodynamic theory of weak ferromagnetism in antiferromagnetic substances Sov. Phys.—JETP 5 1259–72
[17] Moriya T 1960 Anisotropic superexchange interaction and weak ferromagnetism Phys. Rev. 120 91–8
[18] Romming N et al 2013 Writing and deleting single magnetic skyrmions Science 341 636–9
[19] Graf T, Felser C and Parkin S S P 2011 Simple rules for the understanding of Heusler compounds Prog. Solid State Chem. 39 1–50
[20] Meshcheriakova O et al 2014 Large non-collinearity and spin-reorientation in the novel Mn_2RhSn Heusler magnet Phys. Rev. Lett. 113 087203
[21] Meshcheriakova O et al 2015 Structural, electronic, and magnetic properties of perpendicularly magnetised Mn_2RhSn thin films J. Phys. D: Appl. Phys. 48 164008
[22] Alijani V et al 2013 Increasing Curie temperature in tetragonal Mn_2RhSn Heusler compound through substitution of Rh by Co and Mn by Rh J. Appl. Phys. 113 063904
[23] Kübler J 2009 Theory of Itinerant Electron Magnetism (Oxford: Oxford University Press)
[24] Kübler J and Felser C 2012 Berry curvature and the anomalous Hall effect in Heusler compounds Phys. Rev. B 85 012405